Crystallization, Morphology, and Electrical Properties of Bio-Based Poly(trimethylene terephthalate)/Poly(ether esteramide)/Ionomer Blends

Toshikazu Kobayashi,[1] Barbara A. Wood,[2] Akio Takemura[3]

[1]Engineering Polymers, DuPont Co., Wilmington, Delaware 19880-0323
[2]Central Research and Development, DuPont Co., Wilmington, Delaware 19880-0323
[3]Laboratory of Polymeric Materials, Department of Biomaterial Sciences, Graduate School of Agricultural and Life Sciences, University of Tokyo, Bunkyo-ku, Tokyo 113-8567, Japan

ABSTRACT: Bio-based poly(trimethylene terephthalate) (PTT) and poly(ether esteramide) (PEEA) blends were prepared by melt processing with varying weight ratios (0–20 wt %) of ionomers such as lithium-neutralized poly(ethylene-*co*-methacrylic acid) copolymer (EMAA-Li) and sodium-neutralized poly(ethylene-*co*-methacrylic acid) copolymer (EMAA-Na). The blends were characterized by differential scanning calorimetry (DSC), dynamic mechanical analysis (DMA), polarized light microscopy (PLM), and transmission electron microscopy (TEM). DSC and PLM results showed that EMAA-Na increased the crystallization rate for PTT significantly, whereas EMAA-Li did not enhance the crystallization rate at all. Specific interactions between PEEA and ionomers were confirmed by DSC and TEM. Electrostatic performance was also investigated for those PTT blends because PEEA is known as an ion-conductive polymer. Here, we confirmed that both sodium and lithium ionomers work as a synergist to enhance the static decay performance of PTT/PEEA blends. Morphological study of these ternary blends systems was conducted by TEM. Dispersed ionomer domains were encapsulated by PEEA, which increases the interfacial surface area between PEEA and the PTT matrix. This encapsulation effect explains the unexpected synergy for the static dissipation performance on addition of ionomers to PTT/PEEA blends. This core–shell morphology can be predicted by calculating spreading coefficient for the ternary blends. © 2010 Wiley Periodicals, Inc. J Appl Polym Sci 119: 2714–2724, 2011

Key words: biopolymers; blends; ionomers; crystallization; morphology

INTRODUCTION

Poly(trimethylene terephthalate) (PTT) is a newly commercialized aromatic semicrystalline polyester with growing applications in fibers, films, and engineering polymers. PTT belongs to the thermoplastic aromatic polyester family, which includes poly(ethylene terephthalate) (PET) and poly(butylene terephthalate) (PBT). DuPont has recently commercialized the Sorona® PTT renewably sourced polymer, which is made by polycondensation as shown in Scheme 1 from 1,3-propanediol (derived from renewable corn sugar) and fossil fuel-derived terephthalic acid (TPA) or dimethyl terephthalate (DMT). The diol component of this polymer, 1,3-propanediol, can be manufactured via a biological fermentation process from corn sugar.[1–4] DuPont and Genencor International have developed a bacterial biocatalyst to convert corn-derived glucose to 1,3-propanediol in a single stage. DuPont and Tate & Lyle have developed the commercial-scale manufacturing process for 1,3-propanediol based on this biocatalyst. Bio-based polymers are generating considerable interest as alternatives to traditional petroleum-based polymers. The polymers and materials derived from mixed sources of renewables and fossil fuels not only have the desired performance but also are drawing a lot of attention from the sustainability point of view. PTT provides all the advantages generally associated with polyesters, including excellent physical and chemical properties, dimensional stability, low moisture absorption, processability with appropriate nucleating agent, and recyclability. Before DuPont introduced bio-based PTT into the market, petroleum-based PTT was commercially available from 1988 to 2009 from Shell Corporation. PTT polymer has been widely studied especially with regard to its fiber properties,[5–8] crystal structure,[9–12] and thermal and crystallization behaviors.[13–19] More recently, PTT/clay nanocomposites,[20–23] PTT/carbon nanotube,[24] and polymer blends such as PTT/PET,[25–27] PTT/PBT,[26,28] PTT/PC,[29–32] PTT/EPDM,[33–35] PTT/LLDPE,[36,37] and PTT/poly(ether imide)[38,39] have been intensively studied. However, very few studies were done for electrical properties for PTT and PTT blends.

Correspondence to: T. Kobayashi (toshikazu.kobayashi@usa.dupont.com).
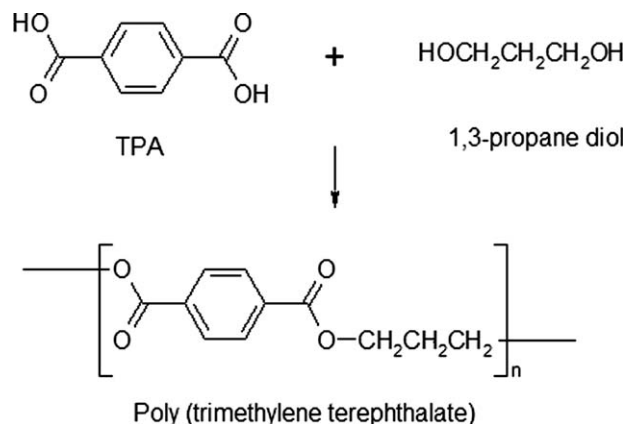
Scheme 1 PTT by condensation reaction from TPA and 1,3-propane diol.

Polymers such as polyesters and polyamides are widely used in various fields such as packaging materials, electrical/electronic parts, and automotive parts. However, the static charge that easily builds up on such molded parts from contact/and or rubbing may create the conditions for sparking and cause an electrostatic discharge, which becomes a serious problem because there may be resulting electrostatic damage to sensitive semiconductor devices and interference with circuit operation. To solve those problems, several approaches have been taken for years such as adding low-molecular-weight surfactant or conductive fillers such as carbon black and carbon fiber. More recently, blending ion-conductive polymers such as poly(ether esteramide) (PEEA) to create better static dissipative polymer systems was studied.[40–42] Here, bio-based PTT and its blends with PEEA and ethylene copolymer-based ionomers such as EMAA-Na and EMAA-Li are investigated in terms of the crystallization, morphology, and electrostatic characteristics.

EXPERIMENTAL

Materials

Poly(trimethylene terephthalate) (PTT; Sorona® by DuPont, intrinsic viscosity: 1.02 dL/g) and poly (ether esteramide) (PEEA; Pelestat® 6321 MFR = 20 g/10 min with 21.18 N at 215°C) used in this work were commercial polymers manufactured by DuPont and Sanyo Chemical Corporation, respectively. The polymers were used without any purification. Sorona® polymer is manufactured from 1,3-propanediol and DMT on a commercial scale using a continuous polymerization process.[43,44] DuPont supplied two kinds of ionomer: poly(ethylene-co-methacrylic acid) (EMAA) copolymer, which was produced by copolymerization of ethylene (85 wt %) and methacrylic acid (15 wt %) at 59% neutralization with so-

dium or lithium. The MFR of EMAA-Na versus EMAA-Li is 0.9 g/10 min versus 1.8 g/10 min, respectively, with 21.18 N at 190°C.

Sample preparation

PTT pellets, PEEA pellets, and other polymer pellets were premixed and extruded on a ZSK 30 twin-screw extruder using a barrel set temperature of 250°C and a screw speed of 300 rpm with the vacuum vent port applied for all formulations. The extruded strand was cut into pellets for injection molding. The extruded pellets were dried for 2 h at 135°C before molding and molded into 7.5 cm × 12.5 cm × 3.2 mm plaques, ASTM tensile test bars, and flexural test bars using an injection molding machine (Sumitomo J-150). The set temperatures for the cylinder and the mold were 250 and 50°C, respectively.

Measurement

Static charge dissipation was measured at 23°C and 50% RH on Static Honest Meter S-4104 (Shishido Shokai, Tokyo, Japan) after applying 10 kV of corona discharge for 60 s. Static Honest Meter is a measuring instrument for attenuation of static electricity. This device is used to electrify the specimen by irradiating it by air ions generated by corona discharges initiated by the device, and then, after the irradiation is stopped, it is used to investigate the decay curve of the charge on the specimen. All samples were conditioned with 23°C and 50% RH for 48 h before the testing.

Transmission electron microscopy (TEM) was performed on ultrathin sections taken from molded tensile bars. To mark the molded surface, the bars were painted with a liquid epoxy mixture, which was cured overnight at 60°C. Cryoultramicrotomy with diamond knives was carried out at −90°C to produce sections of nominal thickness 90 nm. Sections were examined both unstained and after 2-h exposure to RuO$_4$ vapor. Images were obtained using a JEOL 2000FX TEM operated at 200 kV accelerating voltage and recorded on a digital camera.

A Nikon Microphot-FX polarized microscope was used in conjunction with a Linkam THM 600 hot stage. The stage equipped with a Linkam TMS-90 temperature control system allowed samples to be heated and cooled at adjustable rate. The digital video photograph system of PLM includes Panasonic Digital 5000 CCD color video camera, color video monitor, and DVD recorder.

Dynamic mechanical analysis was performed on the samples of 40 mm × 28 mm × 4 mm in size using a dynamic mechanical analyzer (2980 DMA, TA Instruments) under a single cantilever mode in a

TABLE I
Thermal Properties for Various PTT/PEEA Blends

Recipe	Heating				Cooling				
	T_g (°C)	T_{cc} (°C)	ΔH_{cc} (J/g)	T_m (°C)	T_c (°C)	ΔH_c (J/g)	ΔT_c ($T_{onset} - T_c$) (°C)	T_c for PEEA (°C)	Crystalline degree (%)
PTT	45.9	72.4	36.5	229.1	172.6	45.4	17.2	–	31.2
PTT/25% PEEA	44.2	69.6	29.1	228.1	153.7	32.7	32.0	109.9	29.9
PTT/10% E/MAA-Li	44.6	68.3	35.6	227.5	171.5	47.9	18.7	–	36.5
PTT/10% E/MAA-Na	44.1	69.2	1.5	227.3	198.1	50.9	5.0	–	38.8
PTT/25% PEEA/10% E/MAA-Li	44.1	70.3	20.3	227.0	173.5	35.2	18.1	126.3	37.2
PTT/25% PEEA/20% E/MAA-Li	43.5	69.0	19.6	226.9	175.7	26.3	17.7	137.9	32.8
PTT/25% PEEA/10% E/MAA-Na	45.5	–	0	227.6	200.3	37.5	5.7	123.3	39.6
PTT/25% PEEA/20% E/MAA-Na	44.6	–	0	227.6	199.0	30.3	5.2	125.3	37.8

temperature range from −150 to 150°C at a constant heating rate of 2°C/min and at frequency of 2 Hz. All the samples were annealed at 80°C for 30 min before the DMA measurement.

A differential scanning calorimeter, TA Instruments Q1000 MDSC (Modulated DSC) operating in "standard mode," was used to determine the cold crystallization and recrystallization peaks in a melt-quenched sample of the thermoplastic composition. A 10–12 mg sample of the composition was weighed into an aluminum DSC pan, and the sample was heated to 280°C in a DSC for 10 min under nitrogen atmosphere to provide an equilibrated melt sample. The melt sample was removed from the DSC and quick quenched by immersing the sample in liquid nitrogen. The melt-quenched sample was equilibrated at 0°C in the DSC under nitrogen atmosphere, followed by heating at 10°C/min scan rate to 280°C, held at isothermal for 3 min at 280°C, and cooled at 10°C/min scan rate to 30°C while recording the thermal events. The cold crystallization peak (T_{cc}) is the first exothermic peak exhibited in the heating cycle, having a peak height maximum at

about 65–75°C. The enthalpy of the recrystallization peak was measured in Joules per gram (J/g). Peak temperatures of the exothermic curves obtained during the cooling scan were defined as the crystallization temperature (T_c). From the exothermic heat of ΔH, which is caused by crystallization, the crystallinity of PTT is estimated with the following equation:

$$Crysallinity = \Delta H / \Delta H^0, \qquad (1)$$

where ΔH^0 is the fusion of 100% crystalline polymer. Exothermic heats were normalized by the polymer weight percentage in the crystallinity calculations.

RESULTS AND DISCUSSION

Differential scanning calorimetry

The crystallization rate for PTT and PTT blends studied here can be compared by the crystallizing temperature (T_c) and the half peak width of the crystallization peak (ΔT_c). The higher the T_c peak temperature and the narrower the ΔT_c width are, the faster the
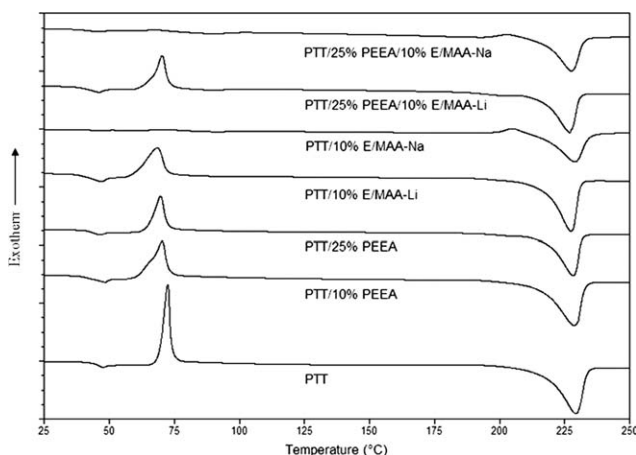

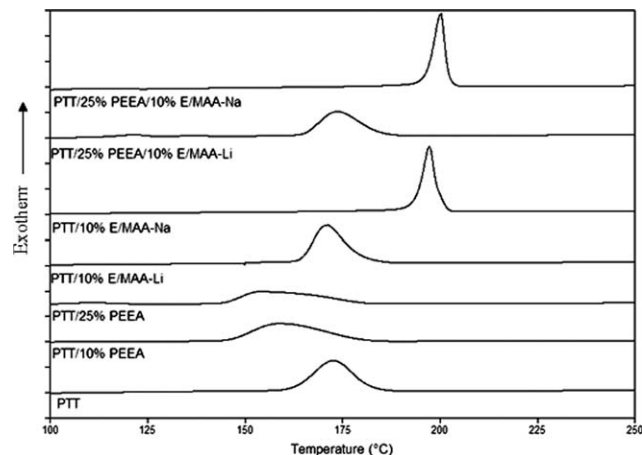**Figure 1** DSC heating scan for PTT and PTT blends.

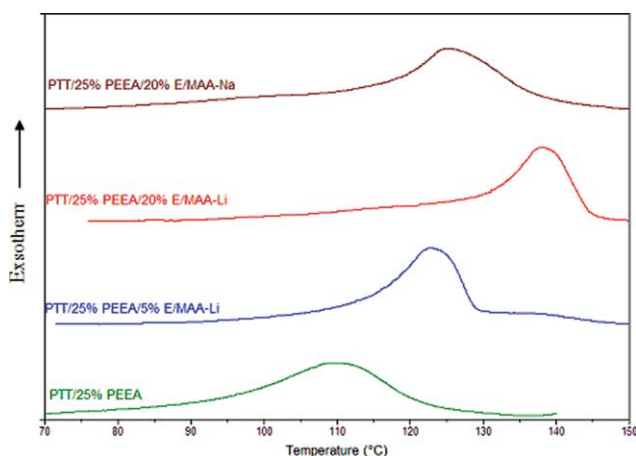**Figure 2** DSC cooling scan for PTT and PTT blends.

Figure 3 DSC cooling scan for PEEA crystallization observation. [Color figure can be viewed in the online issue, which is available at wileyonlinelibrary.com.]

crystallization rate is. Table I lists the analyzed values obtained in the DSC measurements for various PTT blends studied here. The heating scan DSC for the quick-quenched sample by liquid N_2 is shown in Figure 1. The glass transition temperature (T_g) for all the samples is shown around 45°C. T_g for PTT is basically unchanged by blending PEEA, EMAA-Li, or EMAA-Na. The cold crystallization peak on heating up to the melt (T_{cc}), which is observed as exothermic peak, was shown at 72.4°C for neat PTT. The exothermic peak enthalpy (ΔH_{cc}) for the various PTT blends is shown in Table I. There is no exothermic peak for PTT/10% EMAA-Na and PTT/25% PEEA/10% EMAA-Na blends. These blends may have had rapid enough crystallization rate to crystallize during the quenching process with liquid nitrogen, which suggests EMAA-Na enhances the crystallization rate of PTT quite significantly. The cooling scan DSC is shown in Figure 2. The crystallization peak (T_c) for neat PTT can be seen at 172.6°C. When PEEA is added into PTT, T_c shifts to lower temperature (153.7°C for 25% addition) and the
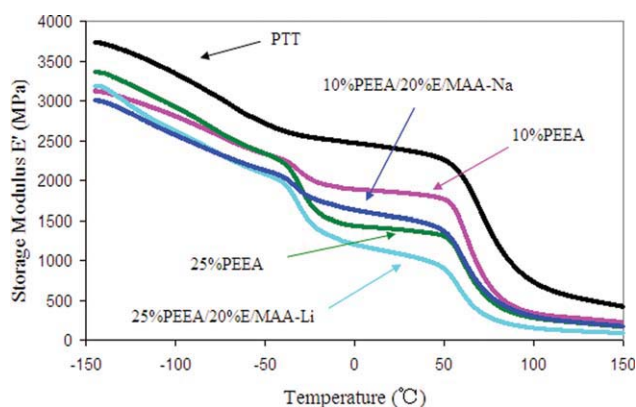

Figure 4 DMA for PTT and various PTT/PEEA blends (E' vs. temperature). [Color figure can be viewed in the online issue, which is available at wileyonlinelibrary.com.]

Figure 5 DMA for PTT and various PTT/PEEA blends (tan δ vs. temperature). [Color figure can be viewed in the online issue, which is available at wileyonlinelibrary.com.]
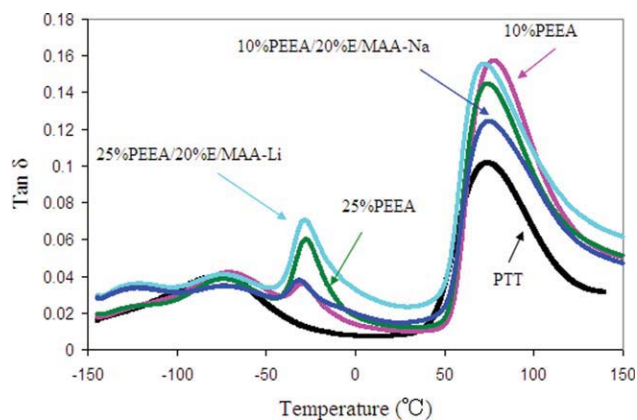
exothermic peak width (ΔT_c: $T_{onset} - T_c$) becomes broader from 17.2 to 32.7°C, which suggested that PEEA retarded the crystallization rate for PTT and acted as a denucleant. On the other hand, PTT blends with EMAA-Na showed higher exothermic peak temperature and narrower peak width (ΔT_c) than neat PTT. T_c for PTT/10% EMAA-Na is seen at 198.1°C, and ΔT_c is only 5°C, which is another evidence that EMAA-Na increases the crystallization rate for PTT. Figure 3 shows the cooling scan from 150 to 70°C where the exothermic peak for PEEA can be observed. T_c for PEEA shifted to higher temperature when either EMAA-Li or EMAA-Na was added into PTT/PEEA blends, which suggested that those ionomers interact with PEEA and enhance the crystallization rate for PEEA domain. The crystallization peak area for PEEA was 3.1–3.3 (J/g), which is much smaller than that of PTT. Figure 3 has a magnification factor of 10× for the Y axis compared to Figure 2 in which T_c for PEEA was not seen. The crystallinity for PTT with the previously described DSC conditions was calculated as 31.2% from the cooling scan, which has good agreement with Zhang.[45] Normalized crystallinity of the PTT portion for various PTT blends is shown in Table I. The value for ΔH^0 in the eq. (1) is 30 kJ/mol = 145.5 J/g as determined by Pyda et al.[46] EMAA-Na addition was confirmed to increase the crystallinity of PTT in the DSC cooling trace (10°C/min.). A 10% addition of EMAA-Na into PTT gave the highest PTT fractional crystallinity, 39.6%, probably because it promotes the crystallization rate for PTT.

Dynamic mechanical analysis

Dynamic mechanical heating scan was performed on bars. Figures 4 and 5 show the storage modulus (E') and tan δ for neat PTT and PTT blends, respectively. The α-relaxation peak that corresponds to the glass
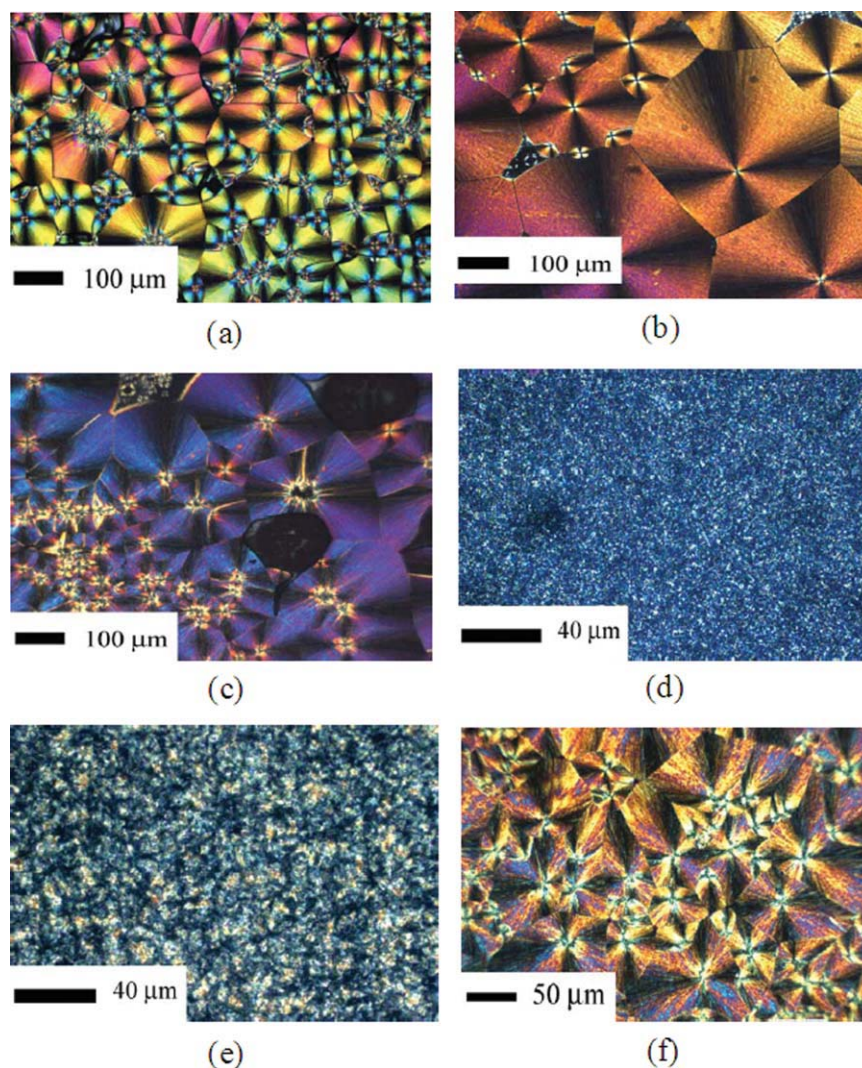
Figure 6 PLM for PTT and PTT blends: (a) PTT, (b) PTT/25% PEEA, (c) PTT/10% EMAA-Li, (d) PTT/10% EMAA-Na, (e) PTT/25% PEEA/5% EMAA-Na, and (f) PTT/25% PEEA/5% EMAA-Li. [Color figure can be viewed in the online issue, which is available at wileyonlinelibrary.com]

transition temperature for neat PTT is observed at 73.8°C, and the β-relaxation for neat PTT can be observed at −74.4°C. Early studies indicated that β-relaxation is produced by joint movement of phenyl rings and carbonyl entities.[47–51] The β-relaxation for PTT is basically unchanged when PEEA, EMAA-Na, and EMAA-Li are added. E' values for PTT blends shown in Figure 4 are significantly lower than that for neat PTT over the temperature range measured here. This result is quite reasonable because both PEEA and ionomers (EMAA-Na and EMAA –Li) are more flexible polymers than PTT. The tan δ peak observed at about −30°C corresponds to T_g of PEEA. With increased PEEA content in PTT, the peak becomes larger. The T_g for PEEA, however, remains unchanged for the PTT blends studied here, which suggests PEEA is not miscible with PTT and ethylene copolymers. One of the unique characteristics for the PTT blends with PEEA

is its static dissipative performance due to the ion conductive nature of PEEA. The T_g of the PEEA domains influences its electrostatic performance, which will be discussed in a separate article.

Spherulite morphology

An optical microscope equipped with a digital video photography system was used to monitor the transmitted light image of the spherulite growth of PTT and PTT blends recrystallized from the melt under controlled conditions.

Figure 6 shows the cross-polarized light optical microscopy (PLM) images spherulites with the distinctive Maltese cross pattern of extinctions. These spherulites were grown by nonisothermal crystallization at the same cooling rate (10°C/min) as DSC after holding the specimen well above the melting point of PTT at 280°C for 3 min with the intent of
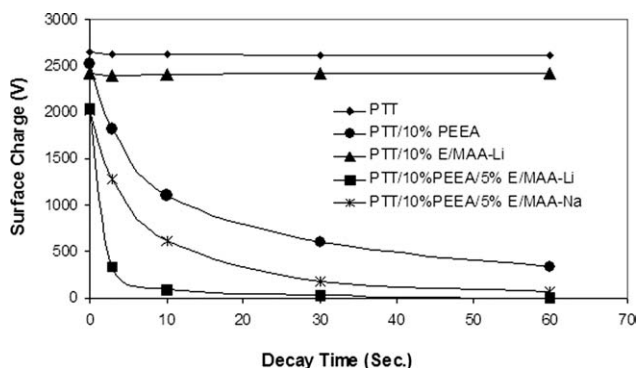
Figure 7 Surface charge decay of PTT and various PTT/PEEA blends.

"erasing" any previous thermal history. The average spherulite size for recrystallized neat PTT is about 100 μm in diameter. PTT/25% PEEA has much larger spherulites than neat PTT, averaging about 300 μm in diameter, which indicates that PEEA retards the crystallization rate for PTT. This PLM image has good agreement with the DSC results. PTT/10% EMAA-Li shows very similar spherulite size compared with the neat PTT. On the other hand, 10% EMAA-Na addition into PTT resulted in significantly smaller spherulites with 1-μm average size, which is explained by the dramatic nucleating effect of EMAA-Na on PTT. In the case of the ternary blend of PTT/25% PEEA/5% EMAA-Li, spherulites averaging about 100 μm in diameter are observed, which is much larger than that of PTT/25% PEEA/5% EMAA-Na.

A number of studies were made in the last few decades to investigate the crystallization acceleration

mechanism of sodium salts in PET.[52–55] The efficient nucleation of PET by sodium salts was reportedly due to the products of sodium carboxylate ends (—COONa), which are created by chemical reactions during the extrusion process between the sodium salts and ester linkage. Sodium carboxylate chain ends precipitate from the polymer melts as ionic clusters and act as seeds in the subsequent crystallization process. EMAA-Na works the same way for PTT nucleation. PTT/25% PEEA/5% EMAA-Na shows spherulites about 5 μm in size, a little larger than the more profusely nucleated PTT/10% EMAA-Na.

Surface charge decay

PEEA is known as an ion-conductive polymer and is commercially available as a polymeric additive to add antistatic characteristics to polymers. We previously investigated electrostatic decay performance for PET/PEEA blends with various polymers such as EMAA, EMAA-Na, EMAA-Li, EMAA-Zn, EMAA-Mg, and polystyrene.[42] We found that the static decay performance for PET/PEEA blends can be drastically improved by adding EMAA-Li and EMAA-Na. Here, we investigate electrostatic decay performance for neat PTT and PTT blends. We chose two ionomers, EMAA-Li and EMAA-Na, to see if they work as synergists to improve the antistatic performance for PTT/PEEA blends.

Surface charge decay curves up to 60 s for the samples were obtained by Static Honest Meter S4104 after applying 10 kV of corona discharge for 1 min. This device is used to electrify the specimen by irradiating it with air ions generated by corona

TABLE II
Surface Charge (V) Decay of Various PTT/PEEA Blends

| QRecipe	Decay time (s)					SDPI (V min)
	0	3	10	30	60	
PTT	2650	2630	2630	2620	2620	2624
PTT/10% PEEA	2520	1820	1100	600	330	795
PTT/25% PEEA	730	60	10	0	0	21
PTT/10% E/MAA-Li	2420	2400	2410	2420	2420	2416
PTT/20% E/MAA-Li	2390	2380	2380	2380	2380	2380
PTT/10% E/MAA-Na	2380	2330	2330	2350	2350	2345
PTT/20% E/MAA-Na	2350	2350	2350	2350	2350	2350
PTT/10% PEEA/5% E/MAA-Li	2040	330	90	30	0	105
PTT/10% PEEA/10% E/MAA-Li	1920	390	50	0	0	84
PTT/10% PEEA/20% E/MAA-Li	1530	160	20	0	0	49
PTT/25% PEEA/5% E/MAA-Li	350	20	10	0	0	10
PTT/25% PEEA/10% E/MAA-Li	290	20	10	0	0	9
PTT/25% PEEA/20% E/MAA-Li	180	20	0	0	0	5
PTT/10% PEEA/5% E/MAA-Na	2030	1280	620	180	70	390
PTT/10% PEEA/10% E/MAA-Na	1880	770	180	40	20	171
PTT/10% PEEA/20% E/MAA-Na	1420	280	40	0	0	67
PTT/25% PEEA/5% E/MAA-Na	460	40	10	0	0	15
PTT/25% PEEA/10% E/MAA-Na	320	30	10	0	0	11
PTT/25% PEEA/20% E/MAA-Na	210	20	0	0	0	6
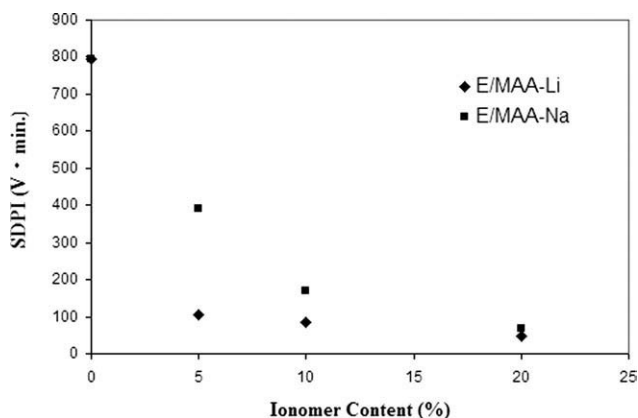
Figure 8 Static decay performance index (SDPI) versus ionomer content when PEEA is 10%.

discharges initiated by the device. After the irradiation is stopped, it is used to investigate the decay curve of the charge on the specimen. Static charge dissipation curve for neat PTT and PTT blends is shown in Figure 7, and the complete set of the data for PTT blends studies here is shown in Table II.

Neat PTT shows no dissipation during measured time of 60 s. The surface charge for PTT/10% PEEA drops from 2520 to 1100 V at 10 s. A 5% addition of EMAA-Li into PTT/10% PEEA gave 90 V surface charge at 10 s, and 20% addition gave only 20 V at 10 s. As previously seen with PET/PEEA blends, adding specific polymers into PTT/PEEA blends in amounts up to 20% induces a synergistic effect on static decay performance because PTT with either 10 or 20% of EMAA-Li does not show any dissipation at all for the measured time period of 60 s. EMAA-Na also works to enhance the static decay performance for PTT/PEEA blends as shown in Figure 7 and Table II. When the loading for PEEA is 25% into PTT, the surface charge was 730 V right after the stop of the irradiation and decayed to 0 V at 30 s. Both 20% loading of EMAA-Li and EMAA-Na into PTT/25% PEEA blend gave 0 V at 10 s with significantly lower initial surface charge.

Static decay performance index (SDPI)

Matsui and Kashiwamura studied the relationship between resistivity, frictional charge, and half dissipation time for antistatic fabricated fiber.[56] In their report, a concept of index of frictional static charge dissipation was proposed to describe the antistatic performance more appropriately. It is the integral of the charge dissipation curve (2) up to 1 min after the applied friction, which is, in other words, the average static charge during 1 min multiplied by 1 min as described in eq. (3). It is known that the dissipation speed decreases when the surface charge becomes small even for the same material. Therefore, half dissipation time tends to become larger when

initial surface charge of the material is low. As good antistatic material tends to have lower initial surface charge with the same applied corona discharge, half dissipation time of the material does not always represent the antistatic performance appropriately, which sometimes makes it difficult to differentiate excellent antistatic material from others. This index is considered as a new method to describe the antistatic performance from the standpoint of both initial surface charge and decay curve. We previously applied Matsui/Kashiwamura concept for describing static charge dissipation to discuss a broader aspect and confirm the effectiveness of static decay performance index (SDPI).[42] The lower the SDPI value, the better static dissipative performance achieved.

$$V = f(t) \tag{2}$$

$$SDPI = \int_0^1 f(t)dt. \tag{3}$$

Figure 8 shows the SDPI for the PTT blends when PEEA content is 10%. Clearly, EMAA-Li works more effectively than EMAA-Na because 5% loading reduced the SDPI from 795 (V min) of PTT/10% PEEA to 105 (V min) for lithium ionomer and 390 (V min) for sodium ionomer. Those SDPI values are significantly low considering that neat PTT, PTT/10% EMAA-Li, and PTT/10% EMAA-Li showed SDPI with 2624 (V min), 2416 (V min), and 2345 (V min), respectively, shown in Table II.

In the DSC, we observed that both EMAA-Na and EMAA-Li enhanced the crystallization rate for PEEA, whereas only EMAA-Na worked as a nucleating agent for PTT. The phenomenon of the nucleation effect for PEEA by those ionomers suggests that there is an interaction between the ionomers and PEEA domains in PTT/PEEA/ionomer ternary blends. The morphological aspect is discussed in the TEM section.

In our previous study, we found that EMAA acid copolymer without any metal cation also works as a synergist for PET/PEEA blends, which suggests that the mechanism of the antistatic synergist is not ion transfer from the ionomer to PEEA but rather morphological interaction in which the PEEA encapsulates dispersed domains of the third polymer. Encapsulation results in higher surface area per unit volume of PEEA compared to PET/PEEA binary blends. However, lithium ionomer works much more effectively than EMAA to decrease the SDPI, especially at low loading. In this case, it is suggested that cation transfer from the ionomer phase to PEEA is enhanced by the morphological interaction between lithium ionomer and PEEA.

Morphology (TEM)

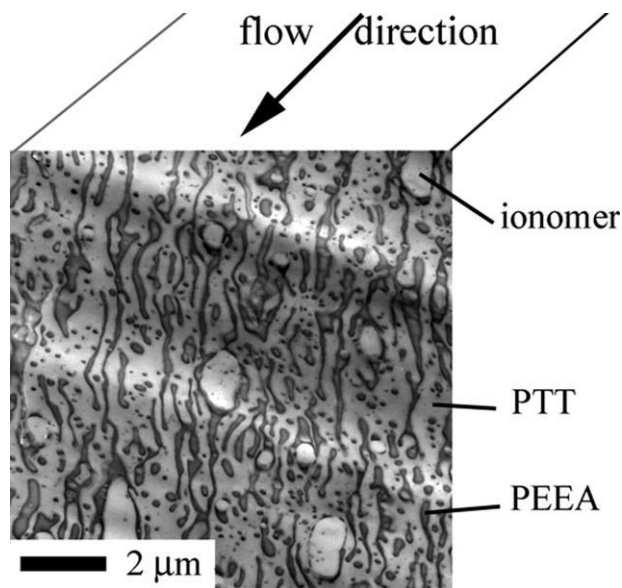A thin cross section of a plaque of PTT/25% PEEA/ 5% EMAA-Li with the PEEA phase stained dark is

Figure 9 TEM of PTT/25% PEEA/5% EMAA-Li (core).

Figure 11 TEM of PTT/25% PEEA/5% EMAA-Na (core).

shown in Figure 9. In this area, sampled well below the molded surface, oriented domains of PEEA up to at least 8 µm long but only 0.1–0.2 µm thick coexist with a few micron-size blobs of the ionomer. Submicron droplets of the PEEA may be the results of oriented worms of plans stretched out past their stability limit. However, most of the blob surface is coated with a layer of PEEA and not in direct contact with the PPT matrix.

In Figure 10, the same molded bar is sampled right at the molded surface and shows the painted-on layer of featureless epoxy. In this subsurface zone, the largest blobs of ionomer are elongated and
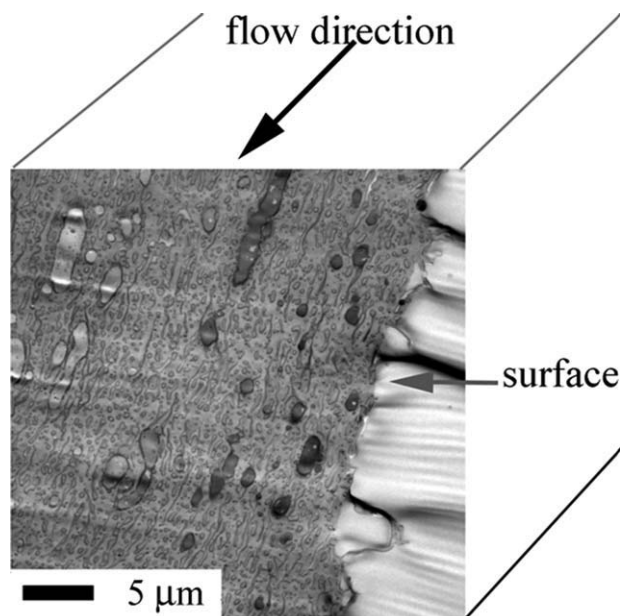
can be up to 6 µm long, with much thinner coating of PEEA than in the center of the bar. PEEA domains are thinner than in the bulk at about 0.05 µm. There is also anomalous staining of the ionomer in the first 10 µm below the bar surface. The enhanced reaction between the ruthenium tetroxide staining agent and ionomer in this zone may reflect higher carboxylic acid content compared with ionomer domains further below the surface and could be the result of the release of lithium cations into the especially thin, high surface area PEEA domains.

A similar composition with sodium instead of lithium ionomer shows only partial encapsulation of ionomer domains by PEEA (Fig. 11). The somewhat weaker interaction between PEEA and EMAA-Na versus PEEA and EMAA-Li is predicted in the next section on spreading coefficients.

Figure 10 TEM of PTT/25% PEEA/5% EMAA-Li (near surface).
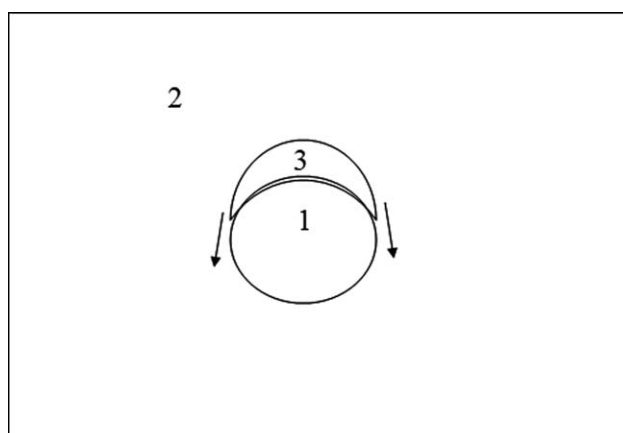
Scheme 2 Schematic diagram showing spreading behavior of one polymer phase on another polymer within a third polymer matrix.

TABLE III
Estimated Surface Tension at the Processing Temperature (250°C)

Polymer	γ (20°C)	Polarity	$-d\gamma/dT$ (mN/m °C)	γ (mN/m)	γ^d (mN/m)	γ^p (mN/m)
PTT	49.2[a]	0.189[a]	0.067[b]	33.79	27.40	6.39
PEEA	46.5[a]	0.157[a]	0.08[b]	28.10	23.69	4.41
E/MAA-Na	43.3[a]	0.034[a]	0.07[c]	27.20	26.26	0.94
E/MAA-Li	37.9[a]	0.032[a]	0.07[c]	21.80	21.11	0.69

[a] Measured by contact angle method.
[b] Sauer.[61]
[c] Estimated—see text for the detail.

Spreading coefficient calculation

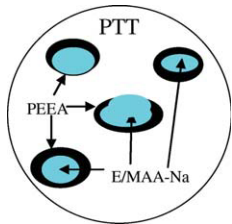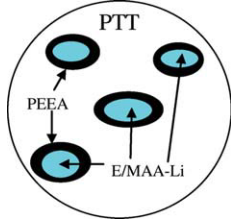$$\lambda_{31} = \gamma_{12} - \gamma_{32} - \gamma_{13}. \qquad (4)$$

The morphology of the ternary blends studied here can be predicted by the calculation of the interfacial tension and the spreading coefficient as shown in (4), where γ_{12}, γ_{32}, and γ_{13} are the interfacial tensions for the each component pair, and λ_{31} is defined as the spreading coefficient for the shell forming component 3 on the core forming component 1. The spreading coefficient λ_{31} must be positive for the component 1 to be encapsulated by the component 3 as shown in Scheme 2. When λ_{31} and λ_{13} are both negative, the dispersed phases of components 1 and 3 will remain separated. In this study, the continuous phase is PTT, whereas PEEA and ionomers will be the dispersed phase. Hobbs et al.[57] and Luzinov et al.[58] investigated three- and four-component polymer blends and showed that the morphology was consistent with the calculated spreading coefficients for each polymer system. Encapsulated morphology was reported for their studied compositions. Nemirovski et al.[59] studied ternary blends consisting of immiscible thermoplastics and thermotropic polymers. The phase morphology was found to be controlled not only by thermodynamic but also by kinetic effects.

$$\gamma_{12} = \gamma_1 + \gamma_2 - 4\left[\frac{\gamma_1^d\gamma_2^d}{\gamma_1^d + \gamma_2^d} + \frac{\gamma_1^p\gamma_2^p}{\gamma_1^p + \gamma_2^p}\right]. \qquad (5)$$

To correlate the phase morphology and the interfacial tension between the constitutive components, the values of γ_{12}, γ_{32}, and γ_{13} have been estimated by using the harmonic mean equation as shown in eq. (5)[60] at the processing temperature. Data for surface tension, polarity (γ^p/γ), and the change in the surface tension with temperature ($d\gamma/dT$) required for the calculation of the interfacial tensions and spreading coefficients are listed in Table III. For PTT, PEEA, EMAA-Na, and EMAA-Li, the surface tension and polarity values were determined by the

contact angle measurements at 20°C using water and methylene iodide. For $d\gamma/dT$ of PTT and PEEA, the value was extracted from the study done by Sauer and Dee.[61] As ($d\gamma/dT$) for EMAA-Na and EMAA-Li was not available, an estimate was made. The variation in surface tension with temperature ($d\gamma/dT$) for most polymers is comparable, 0.06–0.08 mN/m °C.[60,62] The $d\gamma/dT$ for polyethylene and various methacrylic polymers is reported in the range of 0.060–0.067 and 0.059–0.076, respectively.[59] The interfacial tensions and spreading coefficients calculated from the data using 0.07 for $d\gamma/dT$ as estimate value for those ethylene copolymers are shown in Table IV, and the predicted morphology is also illustrated in the table. Spreading of the PEEA phase on both the EMAA-Na and EMAA-Li is shown to be positive in a PTT matrix but with a stronger interaction expected for the lithium ionomer as shown schematically in Table IV by the partial encapsulation of one of the EMAA-Na domains versus complete encapsulation of all EMAA-Li domains. Similarly, the negative spreading coefficient for the ionomers on PEEA is more strongly negative for the lithium

TABLE IV
Estimated Spreading Coefficients at 250°C

Dispersed phase	Matrix polymer	λ (mN/m)	Predicted morphology
PEEA on E/MAA-Na	PTT	1.1	
E/MAA-Na on PEEA	PTT	−5.8	
PEEA on E/MAA-Li	PTT	1.9	
E/MAA-Li on PEEA	PTT	−7.6	

ionomer, and we did not observe such encapsulation in the TEM images.

This explains TEM observation of ionomers encapsulated by PEEA in the core area of the molded parts. These spreading coefficients exhibit good agreement with our TEM observations, but actual extrusion and molding process do not necessarily give thermodynamically equilibrium morphologies. Also, very high orientation of dispersed-phase domains in the surface of the molded parts obscures the observation of completely encapsulated core–shell morphology.

CONCLUSIONS

Bio-based PTT and PTT blends with PEEA, EMAA-Li, and EMAA-Na were studied in terms of the crystallization, spherulite morphology by PLM, dynamic mechanical properties, multicomponent morphology by TEM, and electrostatic characteristics. DSC and PLM suggest significant nucleation and crystallization rate enhancement is achieved for PTT by EMAA-Na addition. However, as previously observed for PET, the lithium ionomer does not enhance PTT nucleation and crystallization. The T_g for PTT and PEEA did not change for the blends studied here, as expected for immiscible ternary blends. SDPI, a convenient figure of merit for comparing different polymeric materials, was calculated from the electrostatic dissipation curve, and it was confirmed that PEEA worked effectively to reduce the SDPI for PTT. Lithium- and sodium-neutralized EMAA worked as synergists to enhance the antistatic performance for PTT/PEEA blends.

Morphological study of these ternary blends system was conducted by TEM. Interfacial segregation of PEEA to domains of EMAA-Li and EMAA-Na was observed at the center of the molded samples. Ionomer domains were partially or completely encapsulated by PEEA. This core–shell morphology, which can be predicted by the spreading coefficient of PEEA onto ionomer domains, explains the synergistic effect for the static decay performance.

References

1. Emptage, M.; Haynie, S.; Laffend, L.; Pucci, J.; Whited, G. Eur. Pat. EP 1204755 (2001).
2. Whited, G. M.; Bulthuis, B.; Trimbur, D. E.; Gatenby, A. A. Eur. Pat. EP 1076708 (1999).
3. Burch, R. R.; Dorsch, R. R.; Laffend, L. A.; Nagarajan, V. Int. Pat. WO 0111070 (2001).
4. Kurian, J. V. J Polym Environ 2005, 13, 159.
5. Grebowicz, J. S.; Brown, H.; Chuah, H. H.; Olvera, J. M.; Wasiak, A.; Sajkiewicz, P. Polymer 2001, 42, 7153.
6. Wu, J.; Schultz, J. M.; Samon, J. M.; Pangelinan, A. B.; Chuah, H. H. Polymer 2001, 42, 7161.
7. Wu, G.; Li, H. W.; Wu, Y. Q.; John, A. Polymer 2002, 43, 4915.
8. Shu, Y. C.; Hsiao, K. J. Eur Polym J 2006, 42, 2773.
9. Ho, R. M.; Ke, K. Z.; Chen, M. Macromolecules 2000, 33, 7529.
10. Wang, B. J.; Christopher, Y. L.; Jennifer, H.; Stephen, Z. D. C.; Phillip, H. G. Polymer 2001, 42, 7171.
11. Chen, M.; Chen, C. C.; Ke, K. Z.; Ho, R. M. J Macromol Sci Phys 2002, 41, 1063.
12. Yun, J. H.; Kuboyama, K.; Chiba, T.; Ougizawa, T. Polymer 2006, 47, 4831.
13. Chung, W. T.; Yeh, W. J.; Hong, P. D. J Appl Polym Sci 2002, 83, 2426.
14. Chuah, H. H. Polym Eng Sci 2001, 41, 308.
15. Hong, P. D.; Chung, W. T.; Hsu, C. F. Polymer 2002, 43, 3335.
16. Srimoaon, P.; Dangseeyun, N.; Supaphol, P. Eur Polym J 2004, 40, 599.
17. Chuang, W. T.; Hong, P. D.; Chuah, H. H. Polymer 2004, 45, 2413.
18. Xue, M. L.; Yu, Y. L.; Sheng, J.; Chuah, H. H. J Macromol Sci Phys 2005, 44, 531.
19. Xue, M. L.; Sheng, J.; Yu, Y. L.; Chuah, H. H. Eur Polym J 2004, 40, 811.
20. Liu, Z.; Chen, K.; Yau, D. Eur Polym J 2003, 39, 2359.
21. Ou, C. F. J Polym Sci Part B: Polym Phys 2003, 41, 2902.
22. Liu, Z.; Chen, K.; Yau, D. Polym Test 2004, 23, 323.
23. Mishra, J. K.; Chang, Y. W.; Choi, N. S. Polym Eng Sci 2007, 47, 863.
24. Xu, Y.; Jia, H. B.; Piao, J. N.; Ye, S. R.; Huang, J. J Mater Sci 2008, 43, 417.
25. Chung, G. S.; Choi, K. R.; Lin, K. Y.; Kim, B. C. Polym Mater Sci Eng 2001, 84, 501.
26. Kuo, Y. H.; Woo, E. M. Polym J 2003, 35, 236.
27. Supaphol, P.; Dangseeyun, N.; Thanomkiat, P.; Nithitanakul, M. J Polym Sci Part B: Polym Phys 2004, 42, 676.
28. Supaphol, P.; Dangseeyun, N.; Srimoaon, P.; Nithitanakul, M. Polym Test 2004, 23, 175.
29. Xue, M. L.; Sheng, J.; Chuah, H. H.; Zhang, X. Y. J Macromol Sci Phys 2004, 43, 1045.
30. Lee, L. T.; Woo, E. M. Colloid Polym Sci 2004, 282, 1308.
31. Oh, S. J.; Chae, D. W.; Lee, H. J.; Kim, B. C. Polym Mater Sci Eng 2001, 84, 621.
32. Bae, W. J.; Jo, W. H.; Park, Y. H. Macromol Res 2002, 10, 145.
33. Ravikumar, H. B.; Raganathaiah, C.; Kumaraswamy, G. N.; Thomas, S. Polymer 2005, 46, 2372.
34. Aravind, I.; Albert, P.; Ranganathaia, C.; Kurian, J. V.; Thomas, S. Polymer 2005, 45, 4925.
35. Ravikumar, H. B.; Ranganathaiah, C. Polym Int 2005, 54, 1288.
36. Jafari, S. H.; Asadinezhad, A.; Yavari, A.; Khonakdar, H. A.; Bohme, F. Polym Bull 2005, 54, 417.
37. Jafari, S. H.; Yavari, A.; Asadinezhad, A.; Khonakdar, H. A.; Bohme, F. Polymer 2005, 46, 5082.
38. Kuo, J. M.; Woo, E. M.; Kuo, T. Y. Polym J 2001, 33, 920.
39. Huang, J. M.; Chang, F. C. J Appl Polym Sci 2002, 84, 850.
40. Fukunaga, K.; Maeno, T. J Electrostatics 1997, 40/41, 431.
41. Kobayashi, T.; Wood, B. A.; Takemura, A.; Ono, H. J Electrostatics 2006, 64, 377.
42. Kobayashi, T.; Wood, B. A.; Takemura, A.; Ono, H. Polym Eng Sci 2008, 48, 2247.
43. Chang, J. C.; Kurian, J. V.; Miller, R. W. U.S. Pat. 7,033,530 (2006).
44. Giardino, C. J.; Griffith, D. B.; Ho, C.; Howell, J. M.; Watkins, M. H.; Duffy, J. J. U.S. Pat. 6,353,062 (2002).

45. Zhang, J. J Appl Polym Sci 2004, 91, 1657.
46. Pyda, M.; Boller, A.; Grebowicz, J.; Chuah, H.; Lebedev, B. V.; Wunderlich, B. J Polym Sci Part B: Polym Phys 1998, 36, 2499.
47. Gonzalez, C. C.; Perena, J. M.; Bello, A. J Polym Sci Part B: Polym Phys 1988, 26, 1397.
48. Kalakkunnath, S.; Kalika, D. S. Polymer 2006, 47, 7085.
49. Mackintosh, A. R.; Liggat, J. J. J Appl Polym Sci 2004, 92, 2791.
50. Maxwell, A. S.; Monnerie, L.; Ward, I. M. Polymer 1998, 39, 6851.
51. Corrales, T.; Peinado, C.; Bosch, P.; Catalina, F. Polymer 2004, 45, 1545.
52. Garcia, D. J Polym Sci Polym Phys Ed 1984, 22, 2063.
53. Legras, R.; Dekoninck, J. M.; Vanzieleghem, A.; Mercier, J. P. Polymer 1986, 27, 109.
54. Dekoninck, J. M.; Legras, R.; Mercier, J. P. Polymer 1989, 30, 910.
55. Mercier, J. P. Polym Eng Sci 1990, 30, 270.
56. Matsui, M.; Kashiwamura, T. Sen-I Gakkaishi 1993, 49, 421.
57. Hobbs, S. Y.; Dekkers, M. E.; Watkins, V. H. Polymer 1988, 29, 1598.
58. Luzinov, I.; Xi, K.; Pagnoulle, C.; Huynh-Ba, G.; Jerome, R. Polymer 1999, 40, 2511.
59. Nemirovski, N.; Siegmann, A.; Narkis, N. J Macromol Sci Phys 1995, 34, 459.
60. Wu, S. J Polym Sci Part C: Polym Symp 1971, 34, 19.
61. Sauer, B. B.; Dee, G. T. Macromolecules 2002, 35, 7024.
62. Wu, S. Polymer Interface and Adhesion; Marcel Dekker, Inc.: New York, 1982; p 67.